Diffusion of Small Molecules in Metal Organic Framework Materials

Pieremanuele Canepa,[1] Nour Nijem,[2] Yves J. Chabal,[2] and T. Thonhauser[1,*]

[1]*Department of Physics, Wake Forest University, Winston-Salem, North Carolina 27109, USA*

[2]*Department of Materials Science and Engineering, University of Texas at Dallas, Texas 75080, USA*

(Received 12 October 2012; published 9 January 2013)

Ab initio simulations are combined with *in situ* infrared spectroscopy to unveil the molecular transport of H_2, CO_2, and H_2O in the metal organic framework MOF-74-Mg. Our study uncovers—at the atomistic level—the major factors governing the transport mechanism of these small molecules. In particular, we identify four key diffusion mechanisms and calculate the corresponding diffusion barriers, which are nicely confirmed by time-resolved infrared experiments. We also answer a long-standing question about the existence of secondary adsorption sites for the guest molecules, and we show how those sites affect the macroscopic diffusion properties. Our findings are important to gain a fundamental understanding of the diffusion processes in these nanoporous materials, with direct implications for the usability of MOFs in gas sequestration and storage applications.

DOI: 10.1103/PhysRevLett.110.026102 PACS numbers: 68.43.Bc, 68.43.Mn, 84.60.Ve

Distressing scenarios of fossil-fuel shortages and greenhouse effects have intensified scientific efforts in seeking innovative materials for energy storage and capture of greenhouse gases. Due to their vast range of tunable properties, metal organic framework (MOF) materials are outstanding candidates to address both issues. They can have large hydrogen-storage capacities, surpassing the U.S. Department of Energy (DOE) storage targets [1–3], and have even been declared DOE's top priority at its 2012 Hydrogen and Fuel Cells Program Annual Review Meeting [4]. On the other hand, due to their large CO_2 uptakes [5,6], MOFs are also interesting for carbon-capture applications. These qualities, combined with their low production cost, have made MOFs the target of many studies, focusing mostly on their adsorption properties [2,3,7–9]. However, their performance for practical storage and capture applications also critically depends on the diffusion and interaction of gases (e.g., with water) in the MOF environment, which are currently poorly understood [6,10,11].

To address this issue and elucidate the diffusion process of small molecules in the nanopores of MOFs, we use a combination of *ab initio* simulations and *in situ* infrared (IR) spectroscopy. Specifically, we study the diffusion of H_2, CO_2, and H_2O in MOF-74-Mg and investigate the role of water on diffusion of small molecules. We focus on this particular MOF, as it has attracted a lot of attention due to its enhanced reactivity with small molecules, caused by the exposure of open metal sites in its nanopores. Britt *et al.* [6] have shown that MOF-74-Mg is extremely efficient in capturing CO_2, compared to isostructural MOFs with other metal sites such as Zn, Mn, Fe, Co, Ni, and Cu.

To model the molecular diffusion in the MOF structure, we use climbing-image nudged elastic band (NEB) [12] simulations coupled with density functional theory, as implemented in QUANTUM ESPRESSO [13]. To correctly capture the weak van der Waals (vdW) forces—which are critical in this study—we use the truly nonlocal functional vdW-DF [14–16], which has already been successfully applied to a number of related studies [17–21]. We use ultrasoft pseudopotentials with wave function and density cutoffs of 480 eV and 4800 eV, respectively. Tests show that Γ-point calculations are sufficient and yield total energies converged to within 5 meV with respect to denser k-point meshes; however, energy *differences*—important for our diffusion barriers—are converged to within less than 1 meV. The self-consistency tolerance was set to 1.4×10^{-10} eV and during optimizations the total forces were relaxed to less than 2.6×10^{-4} eV/Å. We started from the experimental MOF-74-Mg structure, optimizing the internal parameters and keeping the lattice constants fixed to the hexagonal structure with space group $R\bar{3}$ and $a = 25.8810$ Å and $c = 6.8789$ Å [22].

We begin by revisiting the binding characteristics of H_2, CO_2, and H_2O in the MOF framework, which serves here as background for explaining the molecular transport—recent theoretical [23–25] and experimental [24–28] work has fully explored and clarified both origin and nature of the "static" adsorption interactions of H_2 and CO_2 in MOF-74. Our calculated adsorption energies ΔE are given in Table I for two different loadings: (i) low loading, one molecule per cell, and (ii) high loading, six molecules per cell completely saturating all available metal sites (see Fig. 1(a and a') for a graphical representation of these loadings). From the computed vibrational frequencies (see below) we obtain the thermal and zero-point energy (ZPE) corrections to the adsorption energy, allowing for a more accurate comparison to measured adsorption heats. But we find that neither of these corrections has a large effect in our case. Overall, we find very good agreement with the experimental adsorption energies of -0.11 ± 0.003 eV for H_2 [27] and -0.49 ± 0.010 eV for CO_2 [24], attesting to the importance of correctly including

TABLE I. Adsorption energy ΔE of molecules in MOF-74-Mg in eV, and adsorption energies corrected for the zero-point energy (ΔE_{ZPE}) and thermal contribution (ΔH_{298} at 298 K).

Molecule	Loading	ΔE	ΔE_{ZPE}	ΔH_{298}
H_2	1	−0.15	−0.15	−0.15
	6	−0.16	−0.16	−0.16
CO_2	1	−0.50	−0.49	−0.50
	6	−0.50	−0.49	−0.50
H_2O	1	−0.79	−0.76	−0.76
	6	−0.76	−0.73	−0.73

van der Waals interactions in these simulations. The 0.03 eV decrease of ΔE for H_2O in the high-loading situation is linked to the intermolecular repulsions between hydrogen atoms of H_2O adsorbed on adjacent Mg sites. This is also evident from the intermolecular distance $d_{HHO...Mg\text{-}MOF}$, which increases from 2.197 Å for the low-loading case to 2.232 Å for the high-loading case. As a result of the large dipole moment of water (1.9 Debye), it binds very strongly [2]. Thus, water is thermodynamically much more likely to occupy metal sites, significantly reducing the MOF's adsorption capabilities toward H_2 and CO_2, with tremendous importance for storage and capture applications.

While the uncoordinated Mg sites are the most attractive sites, secondary binding sites also exist, which only become occupied at lower temperatures (or high pressures). Recent neutron diffraction experiments isolated such a secondary binding site for CO_2 in MOF-74-Mg [28], where the CO_2 binds to the carboxylate group of the linker. The experimental geometry of this site is well reproduced by our vdW-DF calculations [25]. For very high loading, i.e., 12 CO_2 molecules per unit cell (occupying the primary and secondary sites) the intermolecular repulsions decrease the average ΔE to −0.48 eV.

Vibrational frequencies are a prerequisite to estimate the preexponential factor in the Arrhenius transport equation. We report here the calculated *change* in IR frequency between the gas-phase molecules and the molecules adsorbed in the MOF. In the mono-adsorbed cases we find $\Delta\nu_{H_2} = -30\ \mathrm{cm}^{-1}$, $\Delta\nu_{CO_2} = -13\ \mathrm{cm}^{-1}$, and $\Delta\nu_{H_2O} = -103\ \mathrm{cm}^{-1}$, in excellent agreement with our experimental observations of $-36\ \mathrm{cm}^{-1}$, $-8\ \mathrm{cm}^{-1}$, and $-99\ \mathrm{cm}^{-1}$. Experimentally, there is a small difference in frequency change between low and high loading, resulting in a redshift of $-3\ \mathrm{cm}^{-1}$ and $-15\ \mathrm{cm}^{-1}$ for the asymmetric stretch mode of CO_2 and H_2O (see Supplemental Material [29]). Computationally, we find $\Delta\nu_{CO_2} = -1\ \mathrm{cm}^{-1}$ and $\Delta\nu_{H_2O} = -18\ \mathrm{cm}^{-1}$, in excellent agreement with experiment.

We now move our discussion to the key results of this Letter: The molecular transport in MOF-74-Mg. To study this aspect, we consider the four diffusion mechanisms depicted in Fig. 1. In mechanism (a), a molecule hops circularly from one Mg^{2+} site to its adjacent one. Note that this mechanism is not responsible for molecular transport *into* the MOF, but nevertheless it is an important process for redistributing the load. In mechanism (b), one molecule hops longitudinally (along the c axis) from one Mg^{2+} to the equivalent one in the next unit cell. In mechanism (c), one molecule moves longitudinally through MOF-74 fully loaded with the same type of molecule. And finally, in mechanism (d), one molecule preadsorbed on a Mg^{2+} site moves through a barrier made by six molecules and then binds again at the equivalent site two unit cells further down. We consider those the fundamental diffusion mechanisms that control the macroscopic molecular transport in MOF-74-Mg. Other paths by good approximation are superpositions of the ones discussed here. Mechanism (c) simulates real diffusion and is responsible for penetration deep into the MOF, once the surface is fully saturated. Mechanism (d) simulates the kinetic barrier that a preadsorbed molecule must overcome when the adjacent available metals sites have already been saturated, i.e., obstructing the flux of an incoming molecule. Note that co-diffusion cases are not considered here. For the study of mechanism (a) we used the hexagonal primitive cell with 54 atoms. For mechanism (b), (c), and (d)—requiring a longitudinal displacement of the molecule along the c axis—we employed a supercell containing 108 atoms, expanded along the c axis, making these calculations very challenging.

Figure 2, consistently labeled with Fig. 1, shows the calculated diffusion barriers for H_2, CO_2, and H_2O. The barrier heights of all curves, i.e., their maxima, will be referred to as ΔE^D and are collected in Table II. Not surprisingly, looking at the circular hopping mechanism (a), we see that the molecules experience diffusion barriers similar in magnitudes to the adsorption energies at the metal site. For both H_2 and H_2O the diffusion barriers look alike and are found very symmetric. This is not the case for CO_2, which shows a second minimum located at 58% [see Fig. 2(a)]. The local geometry of this minimum is that of the secondary adsorption site detected by neutron diffraction in Ref. [28]. Figure 2(a) shows that the secondary adsorption site becomes only activated when all six Mg^{2+} sites are fully occupied, as the local minimum (5 meV) is too shallow to trap molecules even at very low temperatures. In other words, the secondary binding site only gets occupied under very high loading or pressure. Barriers calculated for mechanism (b) are similar in magnitude to those of mechanism (a); however, they are slightly more asymmetric. We considered mechanism (b) also for situations of low loading (not shown in Fig. 2); i.e., only one molecule occupies the unit cell and hops along the c axis. In this case, all barriers remain similar with the exception of that for water, which increases by approximately 10%, suggesting that the crowded environment helps the molecule extraction via an expulsion mechanism. Not coincidentally, the maximum of the H_2O barrier of

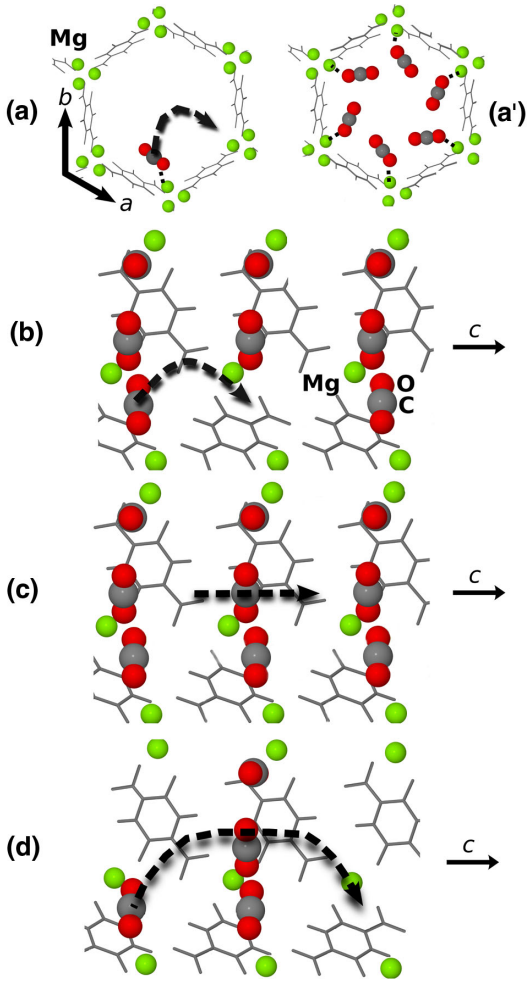

FIG. 1 (color online). Graphical representation of the diffusion mechanisms considered in this study, shown for the case of CO_2. (a) and (a') are views directly along the c axis of the hexagonal MOF-74-Mg cell, where one (low loading) and six CO_2 (high loading) are adsorbed. (b), (c), and (d) are views perpendicular to the c axis. Dashed lines indicate the diffusion paths.

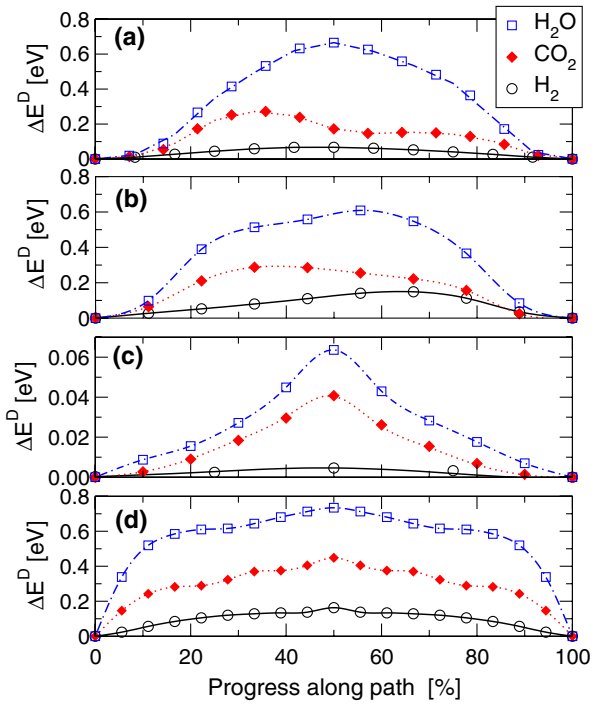

FIG. 2 (color online). Diffusion profiles (in eV) for the diffusion processes of H_2, CO_2, and H_2O in MOF-74-Mg according to the mechanisms in Fig 1.

Fig. 2(b) corresponds to the formation breaking of a lateral hydrogen bond with an oxygen nearby the Mg sites (OOH . . . O-MOF), which decreases its strength passing from low ($d_{\mathrm{OOH...O\text{-}MOF}} = 2.077$ Å) to high loadings ($d_{\mathrm{OOH...O\text{-}MOF}} = 2.138$ Å). It follows that H_2O experiences the largest diffusion barriers and has the highest adsorption affinity to metal sites (see Table I).

Although not immediately obvious from Fig. 2(b), for H_2 there is a small minimum near the 50% mark, which is off the optimized pathway and thus does not show up in the NEB calculation. With the help of additional optimizations near that point, we confirm the presence of a secondary binding site with an adsorption energy of $\Delta E = -0.11$ eV, which is 0.04 eV above the primary binding site (see Table I). The binding pocket is relatively shallow with a depth of approximately 2 meV and the H_2 is clearly "docked" on the "oxygen triangle" formed by the linkers coordinating the Mg sites. Evidence of this binding site was also found in MOF-74-Zn both theoretically [17] and with neutron diffraction experiments [30]. Our calculations thus confirm and quantify the schematic kinetic model (based on experimental evidence) proposed in Fig. 12 of Ref. [26], where the gas-phase H_2 molecules first condense on the metastable second binding site, followed by a gradual migration to the more stable Mg site. Also note that the asymmetric profile for this mechanism suggests that the release of a H_2 molecule from the Mg site is a direct process without intermediate steps. From this analysis we learn that at high pressure and temperature the existence of secondary binding sites assists in the quick redistribution of the molecular load, as molecules entrapped in these sites need less energy to escape from their minima. These sites thus play a crucial role in the load redistribution, affecting the final diffusion properties of incoming molecules. For example, when water is adsorbed at the primary and secondary sites, we can imagine scenarios of high hydrogen bonding reticulation, severely limiting the molecular transport of H_2 and CO_2.

Next, we focus on mechanism (c) and (d), which aim to simulate the molecular flow in the MOF. In mechanism (c), we calculate the barrier for diffusion of a single molecule through a MOF fully loaded with the same type of molecule. Again, water suffers the largest impediment to flow (0.06 eV), while H_2 for this mechanism is almost barrier free (5 meV). Just recently, Bao *et al.* [5] measured ΔE^D for CO_2 and found 0.03 eV, based on experimental CO_2 adsorption isotherms. This is in perfect agreement with our

computed values of 0.04 eV and 0.03 eV (ZPE corrected). Mechanism (d) considers a situation where an adsorbed molecule tries to diffuse further into the MOF, hampered by the presence of a molecular barrier due to other preadsorbed molecules. In this case, the strong electrostatic interaction established by water with the Mg sites imposes a larger diffusion barrier for H_2O when compared to CO_2 and H_2.

We now correlate our diffusion mechanisms at the atomistic level discussed above with our *in situ* time-resolved IR diffusion experiments, which provide information about the macroscopic diffusion of molecules within the MOF scaffold. To this end, we performed IR measurements with diffuse reflectance geometry using a liquid-N_2 cooled Indium Antimonide detector. Approximately 12 mg of sample was mixed with 0.02 g of KBr and inserted into an atmospheric cell from Thermo scientific. The sample was heated *in situ* at 450 K in vacuum for complete desolvation. The pressure was kept constant and changes were monitored as a function of time, while temperature was set to 298 K. IR spectra were recorded every 10 s.

By measuring the asymmetric stretch modes of both CO_2 and H_2O with time, we find that typical MOF loading occurs in two consecutive steps. At the beginning, the guest molecules condense in nanopores on the surface of the MOF, leading to very high loading in those nanopores. From our experiments we conclude that this corresponds to approximately nine molecules per unit cell, effectively clogging the pathways and limiting diffusion of new approaching molecules [25]. This results in a redshift (see Supplemental Material [29]), explained by increasing lateral interactions between adsorbed molecules [25]. Our own calculations of the frequency shift between low and high loading from above confirm that this shift corresponds to high loading. As time progresses, molecules diffuse from highly-loaded pores to low-loading pores deeper inside the bulk of the MOF. As a result, the asymmetric mode returns (with a blueshift; see Supplemental Material [29]) to its original location. This peculiar fluctuation in frequency shifts is a clear signal of a two-states molecular transport mechanism. In particular, the time it takes to return to the original shift—i.e., to get from high to low loading—is characteristic for the guest molecules and provides insight into the diffusion process.

We have performed the above described diffusion experiment for CO_2 and H_2O and find that it takes approximately 2 h for water to diffuse to the low-loading situation, while it takes only 22 min for CO_2 (due to the difficulties of the experiments, we report these times with a large error bar of approximately 25%). More importantly, the ratio of those two times is 5.45. The described experimental situation clearly corresponds to diffusion through mechanism (c) and we can calculate the corresponding ratio using the Arrhenius equation. To this end, we estimated the preexponential diffusion factor using the harmonic transition-state theory (see Supplemental Material [29]) [31]. Using our barrier heights from Table II for CO_2 and H_2O for mechanism (c), we find for the same ratio a value of 5.43, in excellent agreement with experiment. This confirms that we have successfully uncovered transport processes at the atomistic level, which govern the transport processes at the experimentally measured macroscopic level. Ideally, we would like to report other ratios, e.g., for H_2/CO_2, but the corresponding IR experiments involving H_2 are very difficult and results will be published in a longer, forthcoming article.

TABLE II. Diffusion barriers ΔE^D (in eV) of small molecules in MOF-74-Mg. ZPE corrected barriers $\Delta E^D_{\mathrm{ZPE}}$ are given in brackets.

	Diffusion mechanism			
	(a)	(b)	(c)	(d)
H_2	0.07 (0.07)	0.15 (0.15)	0.005 (0.004)	0.16 (0.16)
CO_2	0.27 (0.26)	0.29 (0.28)	0.04 (0.03)	0.45 (0.44)
H_2O	0.67 (0.64)	0.61 (0.58)	0.06 (0.04)	0.73 (0.70)

The fact that water diffuses so much slower than H_2 and CO_2 is to be expected, but of paramount importance for practical applications of MOFs. While the presence of water does not hinder the initial diffusion of other gasses such as H_2 and CO_2 in the noncontaminated MOF structure, high pressure or temperature can affect the delicate thermodynamic equilibrium as incoming H_2O molecules displace preadsorbed H_2 and CO_2 molecules.

In summary, we demonstrate that state of the art *ab initio* NEB simulations, coupled with time-resolved *in situ* IR spectroscopy, provide a complete atomistic understanding of the diffusion processes of three important molecules in MOF-74-Mg for the purpose of hydrogen storage and gas separation. Our theoretical atomistic model for the molecular transport explains experimental IR macroscopic evidence. Furthermore, our calculations clarify the two-states mechanism, observed experimentally, which controls the macroscopic diffusion of these molecules. While the present study only focuses on MOF-74-Mg, it is our belief that the same methodology can be successfully applied to unveil the molecular transport in other MOFs and nanoporous materials, providing further insight into the important question of diffusion as well as a robust theoretical foundation to guide the interpretation of challenging diffusion experiments.

This work was entirely supported by the Department of Energy Grant No. DE-FG02-08ER46491.

*thonhauser@wfu.edu

[1] H. Furukawa, M. A. Miller, and O. M. Yaghi, J. Mater. Chem. **17**, 3197 (2007).

[2] L. J. Murray, M. Dincă, and J. R. Long, Chem. Soc. Rev. **38**, 1294 (2009).

[3] http://www.eere.energy.gov/hydrogenandfuelcells/storage/pdfs/targets_onboard_hydro_storage.pdf.
[4] http://www.hydrogen.energy.gov/annual_review12_proceedings.html.
[5] Z. Bao, L. Yu, Q. Ren, X. Lu, and S. Deng, J. Colloid Interface Sci. **353**, 549 (2011).
[6] D. K. Britt, H. Furukawa, B. Wang, T. G. Glover, and O. M. Yaghi, Proc. Natl. Acad. Sci. U.S.A. **106**, 20 637 (2009).
[7] J. Yang, A. Sudik, C. Wolverton, and D. J. Siegel, Chem. Soc. Rev. **39**, 656 (2010).
[8] J.-R. Li, R. J. Kuppler, and H.-C. Zhou, Chem. Soc. Rev. **38**, 1477 (2009).
[9] J.-R. Li, Y. Ma, M. C. McCarthy, J. Sculley, J. Yu, H.-K. Jeong, P. B. Balbuena, and H.-C. Zhou, Coord. Chem. Rev. **255**, 1791 (2011).
[10] D. K. Britt, D. Tranchemontagne, and O. M. Yaghi, Proc. Natl. Acad. Sci. U.S.A. **105**, 11 623 (2008).
[11] T. G. Golver, G. W. Peterson, B. J. Schindler, D. Britt, and O. M. Yaghi, Chem. Eng. Sci. **66**, 163 (2011).
[12] G. Henkelman, B. P. Uberuaga, and H. Jónsson, J. Chem. Phys. **113**, 9901 (2000).
[13] P. Giannozzi, S. Baroni, N. Bonini, M. Calandra, R. Car, C. Cavazzoni, D. Ceresoli, G. L. Chiarotti, M. Cococcioni, I. Dabo *et al.*, J. Phys. Condens. Matter **21**, 395502 (2009).
[14] M. Dion, H. Rydberg, E. Schröder, D. C. Langreth, and B. I. Lundqvist, Phys. Rev. Lett. **92**, 246401 (2004).
[15] T. Thonhauser, V. R. Cooper, S. Li, A. Puzder, P. Hyldgaard, and D. C. Langreth, Phys. Rev. B **76**, 125112 (2007).
[16] D. C. Langreth, B. I. Lundqvist, S. D. Chakarova-Käck, V. R. Cooper, M. Dion, P. Hyldgaard, A. Kelkkanen, J. Kleis, L. Kong, S. Li, P. G. Moses, E. Murray, A. Puzder, H. Rydberg, E. Schröder, and T. Thonhauser, J. Phys. Condens. Matter **21**, 084203 (2009).
[17] L. Kong, G. Román-Pérez, J. M. Soler, and D. C. Langreth, Phys. Rev. Lett. **103**, 096103 (2009).
[18] Y. Yao, N. Nijem, J. Li, Y. J. Chabal, D. C. Langreth, and T. Thonhauser, Phys. Rev. B **85**, 064302 (2012).
[19] L. Kong, V. R. Cooper, N. Nijem, K. Li, J. Li, Y. J. Chabal, and D. C. Langreth, Phys. Rev. B **79**, 081407(R) (2009).
[20] L. Kong, Y. J. Chabal, and D. C. Langreth, Phys. Rev. B **83**, 121402(R) (2011).
[21] G. Román-Pérez, M. Moaied, J. M. Soler, and F. Yndurain, Phys. Rev. Lett. **105**, 145901 (2010).
[22] H. Wu, W. Zhou, and T. Yildirim, J. Am. Chem. Soc. **131**, 4995 (2009).
[23] L. Valenzano, B. Civalleri, K. Sillar, and J. Sauer, J. Phys. Chem. C **115**, 21777 (2011).
[24] L. Valenzano, B. Civalleri, S. Chavan, G. T. Palomino C. O. Areán, and S. Bordiga, J. Phys. Chem. C **114**, 11 185 (2010).
[25] N. Nijem, P. Canepa, L. Kong, H. Wu, J. Li, T. Thonhauser, and Y. J. Chabal, J. Phys. Condens. Matter **24**, 424203 (2012).
[26] N. Nijem, J.-F. Veyan, L. Kong, H. Wu, Y. Zhao, J. Li, D. C. Langreth, and Y. J. Chabal, J. Am. Chem. Soc. **132**, 14 834 (2010).
[27] W. Zhou, H. Wu, and T. J. Yildirim, J. Am. Chem. Soc. **130**, 15268 (2008).
[28] W. L. Queen, C. M. Brown, D. K. Britt, P. Zajdel, M. R. Hudson, and O. M. Yaghi, J. Phys. Chem. C **115**, 24 915 (2011).
[29] See Supplemental Material at http://link.aps.org/supplemental/10.1103/PhysRevLett.110.026102 for experimental setup, description of infrared spectra, and details on the calculation of the preexponential factors.
[30] Y. Liu, H. Kabbour, C. M. Brown, D. A. Neumann, and C. C. Ahn, Langmuir **24**, 4772 (2008).
[31] G. H. Vineyard, J. Phys. Chem. Solids **3**, 121 (1957).